CARBON letters

Original Articles
Carbon Letters Vol. 23, 30-37 (2017)

Adsorption of Nile Blue A from aqueous solution by different nanostructured carbon adsorbents

Shahryar Abbasi and Hadi Noorizadeh*

Department of Chemistry, Factuly of Science, Ilam University, Ilam, Iran

Article Info

Received 2 February 2017
Accepted 4 May 2017

***Corresponding Author**
E-mail: hadinoorizadeh@yahoo.com
Tel: +98-91-8345-2507

Open Access

DOI: http://dx.doi.org/10.5714/CL.2017.23.030

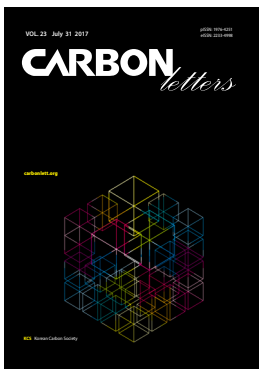

http://carbonlett.org

pISSN: 1976-4251
eISSN: 2233-4998

Abstract

Dyes are widely used in various industries including textile, cosmetic, paper, plastics, rubber, and coating, and their discharge into waterways causes serious environmental and health problems. Four different carbon nanostructures, graphene oxide, oxidized multi-walled carbon nanotubes, activated carbon and multi-walled carbon nanotubes, were used as adsorbents for the removal of Nile Blue A (NBA) dye from aqueous solution. The four carbon nanostructures were characterized by scanning electron microscope and X-ray diffractometer. The effects of various parameters were investigated. Kinetic adsorption data were analyzed using the first-order model and the pseudo-second-order model. The regression results showed that the adsorption kinetics were more accurately represented by the pseudo-second-order model. The equilibrium data for the aqueous solutions were fitted to Langmuir and Freundlich isotherms, and the equilibrium adsorption of NBA was best described by the Langmuir isotherm model. This is the first research on the removal of dye using four carbon nanostructures adsorbents.

Key words: Nile Blue A, graphene oxide, carbon nanotubes, activate carbon, adsorption

1. Introduction

One of the major problems concerning textile wastewater is the colored effluent. The discharge of colored wastewater is not only damaging to the aesthetic nature of the receiving streams but it may also be toxic to aquatic life. The color in the effluent is mainly due to unfixed dye. Azo dyes constitute the largest class of dyes used in industry. Nile Blue A (NBA) is an example of an azo dye. NBA is a potential photosensitizer that can also be used in photodynamic therapy for the treatment of malignant tumors. The cationic NBA dye aggregates in tumor cells, especially in lipid membranes, and is sequestered and concentrated in subcellular organelles. It is also harmful to the respiratory tract if inhaled and an irritant to the skin and eyes [1-3].

Because of the risks they carry, it is necessary to remove organic pollutants using proper treatment methods. A wide variety of treatment methods for the removal of color and dye have been proposed, such as coagulation, filtration, sedimentation, oxidation, membrane separation process, adsorption and so on. Among these processes, the adsorption process is much more competitive than other methods, due to its ready availability, lower cost and the possibility of use in large scales [1].

In the adsorption processes a porous solid (adsorbent) is used to capture the soluble substances present in an aqueous solution (dyes, for instance). Adsorption studies are generally focused on adsorbent selection, and studies which evaluate adsorption performance for dye removal can be commonly found in the literature. Adsorption materials including agro-industrial byproducts [2] chitosan [3] bacterial and fungal biomass [4] minerals [5] activated carbon (AC) [6], multi-walled carbon nanotubes (MWCNTs) [7], oxidized MWCNTs [8] and graphene oxide (GO) [9] among others have already been considered.

AC, MWCNTs, oxidized MWCNTs, and GO are newly emerging carbonaceous nanomaterials. Their characteristic structures and electronic properties make them interact strongly with organic molecules, via non-covalent forces, such as hydrogen bonding, π–π stacking, electrostatic forces, van der Waals forces, and hydrophobic interactions [10,11]. Their nanosized structures also endow them with some advantages including rapid equilibrium rates, high adsorption capacity, and effectiveness over a broad pH range [12].

Carbon nanotubes can be functionalized with various reagents that possess different degrees of oxidation power. In the functionalization process, functional groups (OH, C=O, and COOH) are introduced onto oxidized MWCNTs by sonication for several minutes [13].

In comparison with carbon nanotubes, GO has a higher specific surface area, and its sp^2 hybrid carbon nanostructure can be readily obtained from natural graphite using as easy chemical oxidation–exfoliation–reduction procedure at a low cost [14,15].

In the present study, GO, oxidized MWCNTs, AC, and MWCNTs were used to remove NBA molecules from an aqueous solution. The effects of various parameters were investigated. Based on these studies, the Langmuir and Freundlich isotherm models were used to fit the equilibrium data. Finally, the adsorption kinetics were evaluated.

2. Experimental

2.1. Preparation of carbonaceous materials

The adsorbent materials used for the present work were commercial AC and MWCNTs purchased from Merck (Germany).

2.2. Oxidation of MWCNTs

MWCNTs with lengths ranging from 5–15 μm, with outer diameters of 50–80 nm, inner diameters of 5–10 nm, purity ≥95 were used. For oxidation, 2 g of MWCNTs were placed in a 1 L round bottom flask with a reflux condenser and 300 mL concentrated nitric acid (65%) were added. The mixture was refluxed for 48 h at 120°C, cooled to room temperature, diluted with 500 mL double-distilled water, and vacuum-filtered through filter paper (3 mm porosity; Whatman, UK). Washing was repeated until the pH became neutral, followed by drying in a vacuum oven at 100°C [16].

2.3. Preparation of AC

Chemical activation of the AC was performed by using H_3PO_4 which has long been known and used in the production of AC in industry. According to Teng et al. [17], H_3PO_4 and zinc chloride ($ZnCl_2$) are more common among numerous dehydrating agents [18]. However, they mentioned that $ZnCl_2$ will produce zinc compound contaminants, and thus it is not preferable. Moreover, $ZnCl_2$ will also cause problems of corrosion, inefficient chemical recovery and environmental pollution. Hence, H_3PO_4 was determined to be the better chemical treatment [19]. Double distilled water was stored in brown bottles. The AC was activated by digesting the carbon with the required volume of 4N dilute H_3PO_4 solution, which was then heated at 80°C for 2 h and cooled. After cooling it was washed several times with water in order to remove soluble impurities. The adsorbents were placed in an air oven at a temperature of 120°C for 2 h.

2.4. Synthesis of GO

GO was prepared from natural graphite powder using the modified Hummers method [20]. A mixture of graphite (2 g), $NaNO_3$ (1 g), and concentrated sulfuric acid (100 mL) was stirred for 30 min within an ice bath. Under vigorous stirring, $KMnO_4$ (8 g) was added slowly to the suspension. The rate of addition was carefully controlled to keep the reaction temperature below 10°C. Then the mixture was transferred to an ice bath of 35°C and stirred for three hours, and then 200 mL of H_2O was slowly added. The reaction temperature was rapidly increased to 98°C for 1 h. At this stage, the mixture's color gradually became brown. Water (400 mL) was added to the system. Then 30 mL of H_2O_2 (30%) to reduce the residual permanganate was used. The dark brown mixture gradually changed into a bright yellow color. For purification, the mixture was washed by rinsing and centrifugation with 5% HCl, and then with deionized water several times until the water's pH was close to 7. After filtration and being vacuum dried overnight at room temperature, a dry and solid GO was obtained [21].

2.5. Characterization of carbonaceous materials

The morphology and surface structure of the GO, oxidized MWCNTs, AC, and MWCNTs were examined with a JSM 6700F scanning electron microscope (SEM; JEOL Ltd., Japan). Nitrogen adsorption isotherms at 77 K were determined in a Micrometric ASAP 2000 apparatus (USA). The specific surface area (SSAs) was calculated by the Brunauer-Emmett-Teller (BET) equation, the total pore volume (V_p) was determined at P/P_0=0.98, the adsorption average pore width (4 V/A by BET) (L) was determined by the Barrett-Joyner-Halenda (BJH) method, and micropore volume (V_{micro}) and the external area ($S_{external}$) were determined by the t-method using an appropriate standard isotherm.

N_2 adsorption–desorption experiments showed that AC had a specific surface area of 728 m^2/g. The average pore width (L=2.5 nm) suggests that the AC was a mesoporous adsorbent.

The prepared GO had the highest specific surface area (2030 m^2/g) and pore volume (0.11 cm^3/g), similar to reported values. The average pore width of the GO was 17.3 nm, indicating that GO is a mesoporous material. The formation of a mesoporous structure with a lower surface area may be attributed to the agglomeration of GO layers during the drying process at 100°C, because of the unavoidable van der Waals force between each single sheet of GO.

The results of the BET method showed that the specific surface area of the MWCNTs and oxidized MWCNTs were 165 and 203 $m^2 g^{-1}$, respectively. Also, the average pore diameter and pore volume were 29 nm and 0.17 $cm^3 g^{-1}$ for the MWCNTs, and

36 nm and 0.24 $cm^3 g^{-1}$ for the oxidized MWCNTs, respectively. Due to the larger pore size, the dye molecules can easily diffuse from the surface though the pores of the oxidized MWCNTs [16-18].

2.6. Batch adsorption experiments

Batch adsorption experiments were conducted in a set of 250 mL Erlenmeyer flasks containing adsorbent and 100 mL of MB solution with various initial concentrations. The flasks were agitated in an isothermal water-bath shaker at 120 rpm and 30°C until equilibrium was reached. After decantation and filtration, the equilibrium concentrations of dye in the solution were measured at λ_{max}=600 nm using a UV-visible spectrophotometer. The pH of the solution was adjusted with 1N HCl and 1N NaOH solutions. The amount of dye adsorbed, sorption efficiency (%) and percentage removal of NBA were calculated using Eqs 1 and 2, respectively:

$$\text{Sorption efficiency (\%)} = \frac{C_0 - C_e}{C_0} \times 100 \quad (1)$$

$$q_e = \frac{(C_o - C_e)\,V}{m} \quad (2)$$

where C_0 and C_e (mg/L) are the concentrations of NBA initially and at equilibrium, respectively. V is the volume of the solution (L), m is the weight of adsorbent (g) and q_e (mg/g) is the amount of adsorbed NBA at equilibrium [22]. Finally, the V (V) removal percent (R%) was calculated using Eq. 3:

$$R(\%) = \frac{C_o - C_e}{C_o} \times 100 \quad (3)$$

2.7. Adsorption isotherm

2.7.1. Langmuir isotherm

The Langmuir sorption isotherm was applied to the equilibrium sorption, assuming monolayer sorption on a surface with a finite number of identical sites. The Langmuir equation is written as:

$$\frac{C_e}{q_e} = \frac{C_e}{q_m} + \frac{1}{q_m b_1} \quad (4)$$

The shape of this isotherm can also be expressed in terms of a separation factor (R_L), which is given as follows:

$$R_L = \frac{1}{1 + bC_0} \quad (5)$$

where b is the Langmuir constant (L/mg) related to the affinity of binding sites and the free energy of sorption. q_e is the dye concentration at equilibrium per unit of adsorbent (mg/g). C_e is the dye concentration at equilibrium in solution (mg/L). q_m is the dye concentration when a monolayer forms on the adsorbent (mg/g).

2.7.2. Freundlich isotherm

The Freundlich equation for heterogeneous surface energy systems is given by Eq 6.

$$\ln q_e = \frac{1}{n}\ln C_e + \ln K_F \quad (6)$$

where, K_F is the Freundlich constant (L/mg), and n is the Freundlich constant depending on the intensity of adsorption. The magnitude of the term (1/n) gives an indication of the favorability of the sorbent/adsorbate systems [23].

2.8. Adsorption kinetics

Adsorption is a physiochemical process that involves the mass transfer of a solute from the fluid phase to the adsorbent surface. A study of the kinetics of adsorption is desirable as it provides information about the mechanism of adsorption. The transient behavior of the dye adsorption process was analyzed by using pseudo first order, pseudo second order, and intraparticle diffusion models. A linear form of the pseudo first order model was described by Lagergren.

$$\ln(q_e - q_t) = \frac{\text{h}\; q_e - k_1 t}{2.303} \quad (7)$$

where q_e and q_t are the amounts of NBA adsorbed (mg g^{-1}) at equilibrium and at time t (min), respectively, and k_1 (min^{-1}) is the adsorption rate constant of the pseudo-first order.

The pseudo-second-order kinetic model is expressed as

$$\frac{t}{q_t} = \frac{1}{k_2 q_e^2} + \frac{t}{q_e} \quad (8)$$

where k_2 (g mg^{-1} min^{-1}) is the second order rate constant of adsorption. From the plots of t/q_t against t, q_e and k_2 are evaluated.

2.9. Error analysis

In order to determine the most consistent isotherm and kinetic models for the experimental data, sum of square error (SSE%) and chi-square tests were used:

$$SSE\% = \sqrt{((q_{e,exp} - q_{(e,cal)})/N)} \quad (9)$$

$$X^2 = (q_{(e,exp)} - q_{(e,cal)})^2 / q_{(e,cal)} \quad (10)$$

where $q_{e,exp}$ is the value of the measured q_e, $q_{e,cal}$ is the value of the q_e predicted by the intended model, and N is the number of $q_{e,exp}$.

3. Results and Discussion

3.1. Characterization of the carbon nanostructures

The morphologies and structures of the various carbon nanotubes were observed with a SEM. X-ray diffraction (XRD) was measured with an X-ray diffractometer. SEM images clearly suggested the crystalline tubular structure of nanotubes. The GO film was transparent due its single-atom-layered structure, and had an irregular edge (Fig. 1A). The surface of GO has lots of folds, which come from the scrolling of the GO sheets.

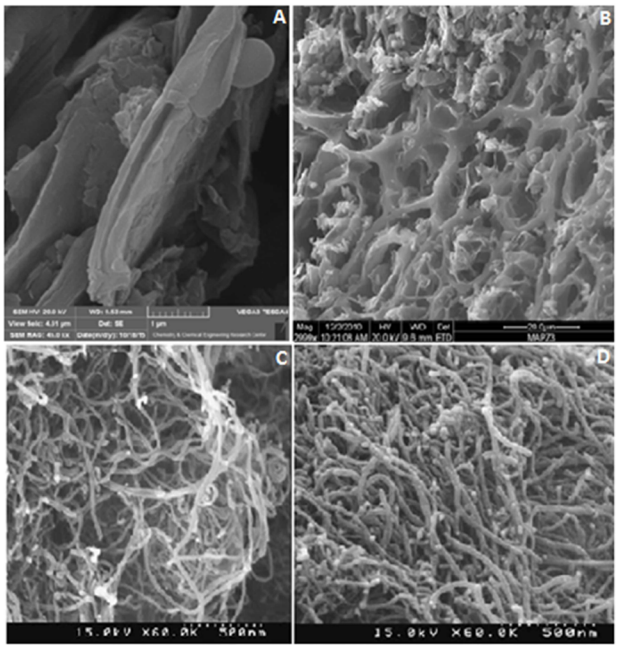

Fig. 1. Scanning electron microscope images of (A) GO, (B) AC, (C) MWCNTs, and (D) oxidized MWCNTs. GO, graphene oxide; AC, activated carbon; MWCNTs, multi-walled carbon nanotubes.

It can be seen that the surface of the AC is very rough, and many pores appear on it (Fig. 1B). Pure MWCNTs form hollow cylinders with long caliber and random states, and agglomerate severely (Fig. 1C). Fig. 1D shows the morphological structure of oxidized MWCNTs. The SEM images clearly reveal the crystalline tubular structure of nanotubes.

The XRD characterization method is used to measure the extent of graphitization, as well as to obtain information about the degree of nanotube alignment. The XRD patterns of the GO nanosheets are shown in Fig. 2A. The diffraction peak at 2θ=26.58 indicates the (002) planes of GO. The distances between the layers of GO are possibly due to the formation of oxygen-containing functional groups, such as hydroxyl, epoxy and carboxyl groups. Accordingly, it can be concluded from the XRD pattern that the graphite powder is almost completely oxidized.

The appearance of a broad diffraction background and the absence of a sharp peak in the AC results reveal a predominantly amorphous structure (Fig. 2B). This is a broad diffraction background corresponding to 2θ=25° in the spectrum, and is a reflection of the 002 plane in the AC structure [24].

Fig. 2C and D show a comparison between the XRD of the MWCNTs and the oxidized MWCNTs. The pattern of the oxidized MWCNTs shows a high intense peak at 2θ=24.6° and a low intense peak at 2θ=43.9°, corresponding to the (002) and (100) reflections, respectively. Compared to the peaks of the MWCNTs, 2θ=25.2° and 2θ=44.0°, these peaks show a downward shift, which is attributed to an increase in the sp^2 C=C layers spacing, and suggests that crystallinity was not lost following the oxidative acid treatment [25].

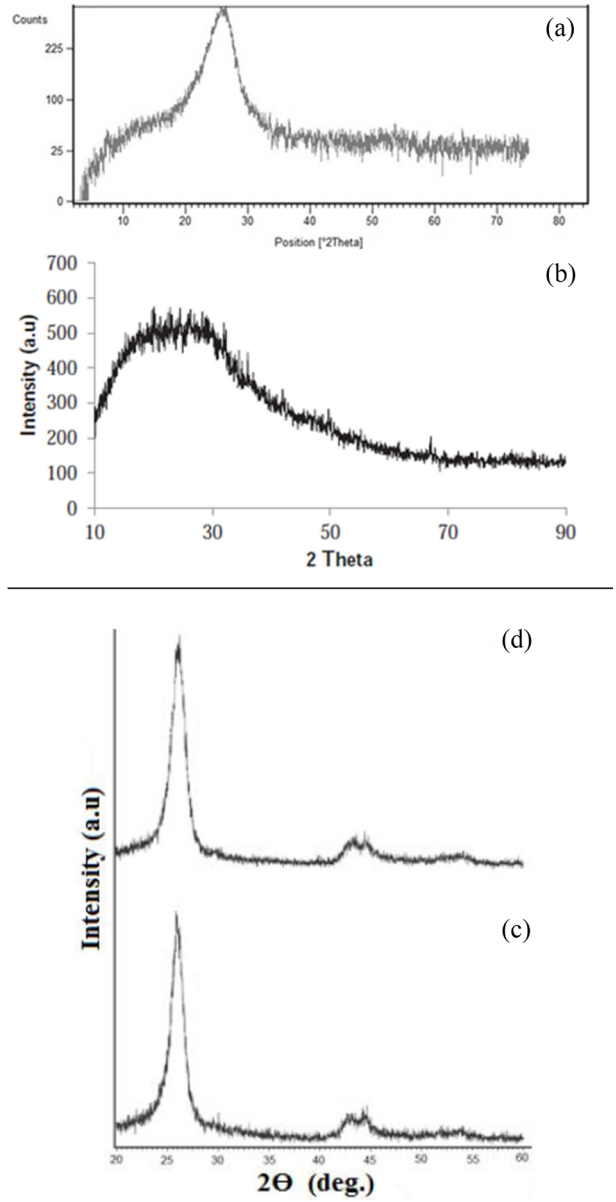

Fig. 2. X-ray diffraction patterns for (A) GO, (B) AC, (C) MWCNTs, and (D) oxidize MWCNTs. GO, graphene oxide; AC, activated carbon; MWCNTs, multi-walled carbon nanotubes.

3.2. The effect of contact time on the removal of NBA dye

The mechanism of transferring an adsorbate mass onto an adsorbent consists of three stages: 1) diffusion of the adsorbate into the liquid layer around the adsorbent; 2) diffusion of the adsorbate into the adsorbent surface; and 3) surface adsorption of the adsorbate on the internal surface of the adsorbent pores.

The effect of contact time on the removal of NBA dye by the four adsorbents in the target solution is shown in Fig. 3. It shows, at all the concentrations used, that as the contact time between the adsorbent and the adsorbate increased, the adsorp-

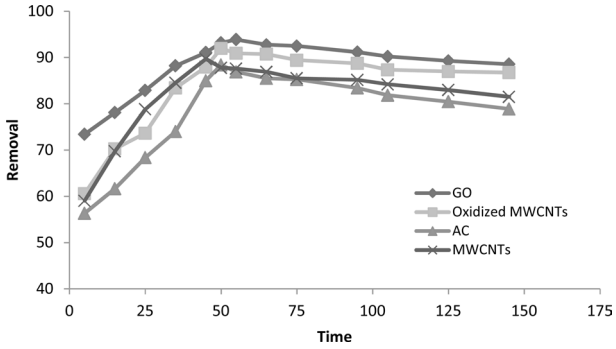

Fig. 3. The effect of contact time on the NBA by GO, oxidized MWCNTs, AC, and MWCNTs. NBA, Nile Blue A; GO, graphene oxide; MWCNTs, multi-walled carbon nanotubes; AC, activated carbon.

tion rate increased too. The highest rate of NBA removal for the GO, oxidized MWCNTs, AC, and MWCNTs took place in the 0–55 minute interval, after which it tapered off. The reason for this performance may be that the dye accessed a high number of vacant binding active sites at the beginning and then gradually covered the binding sites, which reduced the adsorption speed, and in the end an equilibrium was achieved.

In the remaining concentrations, the system was almost constant and did not have much adsorption. GO possessed high removal efficiency because its single-atom-layered structure allows for the speedy attraction of dye molecules.

With their hollow and layered structures and tunable surface chemistry, CNTs may theoretically be a promising third generation of carbonaceous adsorbents.

We systematically investigated the influence of the surface oxidation of the MWCNTs on their adsorption capacity and affinity for the organic compounds in water, and found that surface oxidation of the MWCNTs decreased the surface-area-normalized adsorption capacity of organic compounds significantly, because of the competition of water molecules [27].

3.3. Effect of pH

The pH of the system exerts a profound influence on the adsorptive uptake of adsorbate molecules, presumably due to its influence on the surface properties of the adsorbent and ionization/dissociation of the adsorbate molecule. According to the results in this study, the adsorption percentage of NBA increased when the pH of the aqueous solution was increased from 2.0 to 7.0.

Both the GO and oxidized MWCNTs exhibited very high removal efficiencies, which reached 73.3–93.8% for GO and 69.5–90.2% for oxidized MWCNTs, respectively. Also the dye removal efficiency of the AC and MWCNTs was 61.2–85.5% for the AC and 60.8–87.8% for MWCNTs, respectively in the studied pH range.

The pH_{zpc} (pH of zero net proton charge) is defined here as the pH value at which the net surface charges is equal to zero. pH_{zpc} for the AC, MWCNTs, oxidized MWCNTs and GO were determined to be around 5.3, 4.2, 4.0, and 3.3 respectively [28-30]. At high pH values ($pH>pH_{zpc}$), the surface of the adsorbent is charged negatively and the adsorption of dye molecules increases due to the electrostatic attraction between the surface and the cationic dye molecules. At low pH values ($pH<pH_{zpc}$), since the surface of the adsorbent is charged positively, the expected tendency is a decreasing adsorption of dye, due to the electrostatic repulsion between the cationic dye molecules and the surface of the adsorbent. Altogether, the results show that the adsorption of NBA onto the four adsorbents was not drastically influenced by solution pH.

3.4. Adsorption isotherms

The kinetics of adsorption were studied at various initial dye concentrations. The results of the concentration optimization showed that the adsorption of NBA molecules by GO, oxidized MWCNTs, AC, and MWCNTs increased with their increasing concentration, and reached equilibrium at about 10, 7, 12, and 7 mol/L respectively. The results show that the NBA removal efficiency increases from 40.11% to 93.05% with an increase in adsorbent dose from 0.001 to 0.04 g, and the maximum adsorption was observed at 0.04 g (not shown in this paper). This is because of the increase in the surface area and the availability of more active sites for adsorption. Thus 0.025, 0.03, 0.04, and 0.025 g of GO, oxidized MWCNTs, AC, and MWCNTs, respectively were chosen as the adsorbent dose for all latter experiments in this paper because of higher sorption efficiency and passable sorption capacity.

The results indicated that the pore volume and the average pore diameter of the MWCNTs were less than those of the oxidized MWCNTs. This can be understood by considering the structure change of oxidized MWCNTs on exposure to nitric acid, which can easily break up the MWCNTs into smaller pieces, produce a large amount of defects on their surface and expand the tips, and introduce holes through the MWCNTs [31].

Analyzing the equilibrium data is important for evaluating the adsorption properties of the GO, Oxidized MWCNTs, AC, and MWCNTs adsorbents. The experimental adsorption isotherms of NBA onto the adsorbents were fitted to Langmuir and Freundlich isotherm models (Fig. 4). The isotherm parameters evaluated from the slope and intercept of plots of Ce/qe versus Ce are presented in Table 1. The linear relationships of the plots after modeling the equilibrium data, along with high correlation coefficients, indicate the applicability of the model to the experimental data, and thus the homogeneous nature of

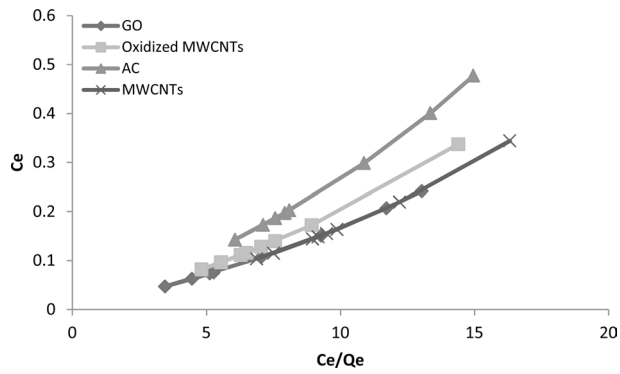

Fig. 4. Langmuir isotherm for the adsorption of NBA onto GO, oxidized MWCNTs, AC, and MWCNTs. NBA, Nile Blue A; GO, graphene oxide; MWCNTs, multi-walled carbon nanotubes; AC, activated carbon.

Table 1. Isotherm parameters of adsorption of NBA onto four adsorbent

Adsorbent	Langmuir				Freundlich		
	b	q_m	R_L	R^2	K_F	n	R^2
GO	0.69	50	0.035	0.995	38.64	4.62	0.961
OMWCNTs	0.46	40	0.352	0.994	32.1	3.49	0.967
AC	0.39	27	0.060	0.994	21.02	3.07	0.963
MWCNTs	0.30	39	0.076	0.989	15.28	2.65	93.8

NBA, Nile Blue A; GO, graphene oxide; OMWCNTs, oxidized multi-walled carbon nanotubes; AC, activated carbon.

Table 2. Pseudo-first-order and -second-order kinetic model parameters for the adsorption of NBA molecules onto GO, oxidized MWCNTs, AC, and MWCNTs

	Pseudo-first-order model						Pseudo-second-order model				
	$q_{e,exp}$	$q_{e,cal}$	K_1	SSE%	χ^2	R^2	$q_{e,cal}$	K_2	SSE%	χ^2	R^2
GO	55.11	28.86	0.025	1.81	23.87	0.601	52.92	0.0152	0.22	0.09	0.998
OMWCNTs	61.32	12.6	0.029	6.09	188.38	0.578	58.5	0.0059	0.28	0.13	0.998
AC	56.69	24.02	0.014	4.08	44.43	0.581	48.66	0.0096	0.80	1.32	0.995
MWCNTs	61.76	9.81	0.007	6.49	275.10	0.488	71.42	0.0196	0.97	1.30	0.997

NBA, Nile Blue A; GO, graphene oxide; OMWCNTs, oxidized multi-walled carbon nanotubes; AC, activated carbon; SSE%, sum of square error.

the tested carbon-based materials. The results show that the four adsorbents have a high affinity for NBA and that the amount of dye adsorbed per unit of adsorbent mass increased as initial dye concentration increased.

The tested carbon-based materials were effective in removing dye at low equilibrium concentrations and reached their maximum adsorption capacity at the highest concentrations.

It was observed that the removal efficiency varied depending on the type of dye and adsorbent applied. The value of R_L shows the type of the isotherm, indicating it is either irreversible (R_L=0), linear (R_L<1), unfavorable (R_L>1) and or favorable (0<R_L<1). According to Table 2, The R_L values were in the range of 0–1, indicating that the sorption of NBA molecules on adsorbents is favorable under the conditions used in this study. The parameters K_F and n indicate the sorption capacity and the sorption intensity of the system, respectively.

Because of its unique nanostructure, graphene has many novel properties, including high surface area, excellent electrical conductivity and electron mobility at room temperature, and it has unique thermal and mechanical properties as well. GO is similar to graphene, but contains oxygen-containing functional groups. In comparison with classical adsorbents such as AC and clay, GO is more attractive because of its favorable physicochemical stability, high selectivity, and structural diversity. Dye is strongly deposited on the GO surface via π–π interactions and cation–π bonding. Large quantities of oxygen atoms are present on the surface of the resulting GO in the forms of epoxy, hydroxyl, and carboxyl groups. The presence of all these functional groups on the GO makes it extremely hydrophilic and allows GO to be effectively applied in aquatic and biological environments.

3.5. Adsorption kinetics

To analyze the kinetic data, pseudo first order and pseudo-second-order kinetic models were applied. The values of k_2 and q_e were evaluated from a linear regression of t/qt versus t and are listed in Table 2. Generally, the adsorption rate was faster at lower dye concentrations; however, the rate coefficients were higher for GO than other adsorbents at each concentration studied. The calculated values for the adsorption capacities ($q_{e,cal}$) agreed well with experimental values ($q_{e,exp}$), confirming that the pseudo-second-order model was suitable for characterizing the NBA adsorption kinetics of the four adsorbents. The linearity of the plots obtained by modeling the kinetics of adsorption had very high correlation coefficients, indicating that the adsorption mechanism of the dyes for GO, oxidized MWCNTs, AC and MWCNTs followed a pseudo-second-order reaction, as shown in Fig. 5. The pseudo-second-order model was successfully applied to evaluate the kinetics of dye adsorption; the same equation was used to fit the adsorption kinetics data at different solution temperatures (not shown in this paper). The low value of the rate constant (k_2) suggests that the adsorption rate decreased with increasing time, and the adsorption rate was proportional to the number of unoccupied sites, as listed in Table 2.

According to the results, the adsorption capacity of NBA onto GO and CNTs was high. The main reason for the high-normalized adsorption capacity of MB onto GO and CNTs can be attributed to the π–π electron donor acceptor interactions with graphene surfaces. NBA has C–C double bonds and contains π electrons. These π electrons can easily interact with the π electrons of benzene rings on the GO and CNT surfaces through π–π electron coupling [32].

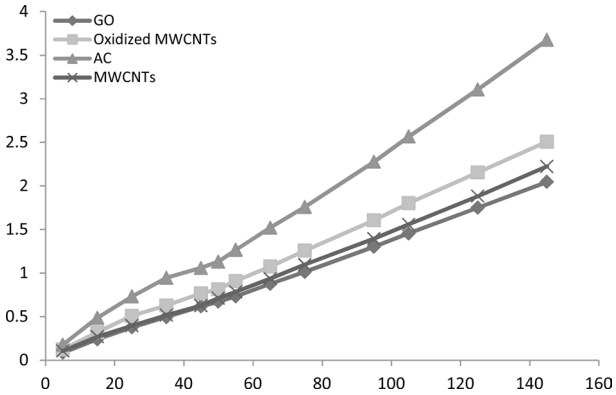

Fig. 5. Pseudo-second-order kinetic plot for the adsorption of NBA onto GO, oxidized MWCNTs, AC, and MWCNTs. NBA, Nile Blue A; GO, graphene oxide; MWCNTs, multi-walled carbon nanotubes; AC, activated carbon.

With the number of aforementioned advantages, including stronger chemical-nanotube interactions, tailored surface chemistry, rapid equilibrium rates, and high sorption capacity, oxidized MWCNTs are considered to be superior sorbents for a wide range of organic chemicals and inorganic contaminants than the conventional AC.

The mechanism behind the strong adsorption of dye on GO is not clear yet. The π–π stacking interaction has always been considered a dominant driving force, and has been used to explain the mechanism of aromatic adsorbates on a graphene surface. At the same time, the cation– π bonding could also be responsible for adsorption. The cation–π bonding is dominated by the cation-induced polarization and electrostatic force between the cation and the permanent quadrupole of the π-electron-rich aromatic structure [33].

3.6. Error analysis

In this study, to determine the best model for predicting adsorption behavior, and to investigate the fitness of different models to the obtained experimental data, statistical analysis methods like the SSE% were used in addition to the application of R^2. The results are presented in Table 2 and Fig. 6. It can be concluded that the pseudo-second-order models had the best goodness of fit, and the SSE% and chi-square for GO was lower, which shows its precision was better than the other adsorbents.

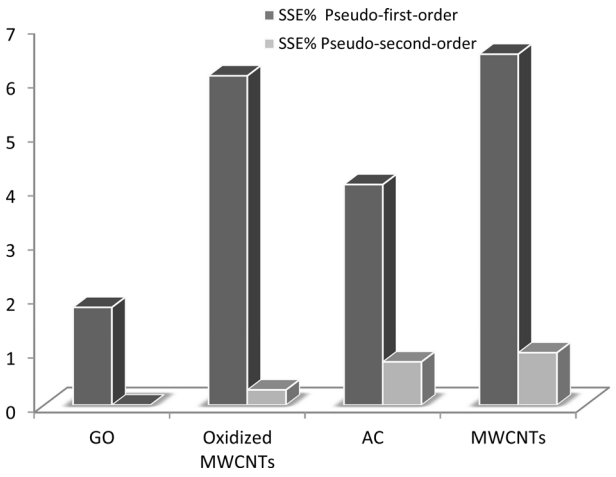

Fig. 6. Comparison of the precision of the different kinetic models. SSE%, sum of square error; GO, graphene oxide; MWCNTs, multi-walled carbon nanotubes; AC, activated carbon.

4. Conclusions

GO, oxidized MWCNTs, AC, and MWCNTs were investigated for removing NBA from aqueous solutions. The adsorbents displayed a well-developed surface and porous structure that was beneficial for the treatment of the dye-contaminated effluents. The four carbon adsorbents exhibited a high adsorptive capacity for NBA under experimental conditions. However, the obtained data revealed that GO demonstrated a better performance for NBA removal than the other carbon nanostructure adsorbents. The isotherm parameters for the Langmuir and Freundlich models were determined and the equilibrium data were best described by the Langmuir isotherm model. The kinetics studies showed that the experimental data can be well fitted by the pseudo second order rate equation. The results indicated that the adsorption of NBA onto the carbonaceous materials was due not only to the large surface area but also to π–π electron donor acceptor interactions and electrostatic attraction between the positively charged dye ions and negatively charged adsorbents.

Conflict of Interest

No potential conflict of interest relevant to this article was reported.

References

[1] Habila MA, ALOthman ZA, Ali R, Ghafar AA, El-Din Hassouna MS. Removal of tartrazine dye onto mixed-waste activated carbon: kinetic and thermodynamic studies. Clean Soil Air Water, **42**, 1824 (2014). https://doi.org/10.1002/clen.201300191.

[2] Vieira AP, Santana SAA, Bezerra CWB, Silva HAS, Chaves JAP, de Melo JCP, da Silva Filho EC, Airoldi C. Kinetics and thermodynamics of textile dye adsorption from aqueous solutions using babassu coconut mesocarp. J Hazard Mater, **166**, 1272 (2009). https://doi.org/10.1016/j.jhazmat.2008.12.043.

[3] Chen CY, Chang JC, Chen AH. Competitive biosorption of azo dyes from aqueous solution on the templated crosslinked-chitosan nanoparticles. J Hazard Mater, **185**, 430 (2011). https://doi.org/10.1016/j.jhazmat.2010.09.051.

[4] Yenikaya C, Atar E, Olgun A, Atar N, Ilhan S, Çolak F. Biosorption study of anionic dyes from aqueous solutions using Bacillus amyloliquefaciens. Eng Life Sci, **10**, 233 (2010). https://doi.org/10.1002/elsc.200900108.

[5] Nassar MM, El-Geundi MS, Al-Wahbi AA. Equilibrium modeling and thermodynamic parameters for adsorption of cationic dyes onto Yemen natural clay. Desalin Water Treat, **44**, 340 (2012). https://doi.org/10.1080/19443994.2012.691701.

[6] Aber S, Sheydaei M. Removal of COD from industrial effluent containing indigo dye using adsorption method by activated car-

bon cloth: optimization, kinetic, and isotherm studies. Clean Soil Air Water, **40**, 87 (2012). https://doi.org/10.1002/clen.201000434.

[7] Gong JL, Wang B, Zeng GM, Yang CP, Niu CG, Niu QY, Zhou WJ, Liang Y. Removal of cationic dyes from aqueous solution using magnetic multi-wall carbon nanotube nanocomposite as adsorbent. J Hazard Mater, **164**, 1517 (2009). https://doi.org/10.1016/j.jhazmat.2008.09.072.

[8] Ghaedi M, Kokhdan SN. Oxidized multiwalled carbon nanotubes for the removal of methyl red (MR): kinetics and equilibrium study. Desalin Water Treat, **49**, 317 (2012). https://doi.org/10.1080/19443994.2012.719355.

[9] Sharma P, Das MR. Removal of a cationic dye from aqueous solution using graphene oxide nanosheets: investigation of adsorption parameters. J Chem Eng Data, **58**, 151 (2013). https://doi.org/10.1021/je301020n.

[10] Pyrzynska K. Carbon nanotubes as sorbents in the analysis of pesticides. Chemosphere, **83**, 1407 (2011). https://doi.org/10.1016/j.chemosphere.2011.01.057.

[11] Yang ST, Chen S, Chang Y, Cao A, Liu Y, Wang H. Removal of methylene blue from aqueous solution by graphene oxide. J Colloid Interface Sci, **359**, 24 (2011). https://doi.org/10.1016/j.jcis.2011.02.064.

[12] Mauter MS, Elimelech M. Environmental applications of carbon-based nanomaterials. Environ Sci Technol, **42**, 5843 (2008). https://doi.org/10.1021/es8006904.

[13] Lee J, Kim M, Hong CK, Shim SE. Measurement of the dispersion stability of pristine and surface-modified multiwalled carbon nanotubes in various nonpolar and polar solvents. Meas Sci Technol, **18**, 3707 (2007). https://doi.org/10.1088/0957-0233/18/12/005.

[14] Zhang L, Li X, Wang M, He Y, Chai L, Huang J, Wang H, Wu X, Lai Y. Highly flexible and porous nanoparticle-loaded films for dye removal by graphene oxide–fungus interaction. ACS Appl Mater Interfaces, **8**, 34638 (2016). https://doi.org/10.1021/acsami.6b10920.

[15] Jayanthi S, Eswar NK, Singh SA, Chatterjee K, Madras G, Sood AK. Macroporous three-dimensional graphene oxide foams for dye adsorption and antibacterial applications. RSC Adv, **6**, 1231 (2016). https://doi.org/10.1039/c5ra19925e.

[16] Atieh MA, Bakather OY, Al-Tawbini B, Bukhari AA, Abuilaiwi FA, Fettouhi MB. Effect of carboxylic group functionalized on carbon nanotubes surface on the of lead from water. Bioinorg Chem Appl, **2010**, 603978 (2010). https://doi.org/10.1155/2010/603978.

[17] Teng H, Yeh TS, Hsu LY. Preparation of activated carbon from bituminous coal with phosphoric acid activation. Carbon, **36**, 1387 (1998). https://doi.org/10.1016/s0008-6223(98)00127-4.

[18] Brunauer S, Emmett PH, Teller, E. Adsorption of gases in multimolecular layers. J Am Chem Soc, **60**, 309 (1938). https://doi.org/10.1021/ja01269a023.

[19] Baccar R, Bouzid J, Feki M, Montiel A. Preparation of activated carbon from Tunisian olive-waste cakes and its application for adsorption of heavy metal ions. J Hazard Mater, **162**, 1522 (2009). https://doi.org/10.1016/j.jhazmat.2008.06.041.

[20] Agorku ES, Mamo MA, Mamba BB, Pandey AC, Mishra AK. Cobalt-doped ZnS-reduced graphene oxide nanocomposite as an advanced photocatalytic material. J Porous Mater, **22**, 47 (2015). https://doi.org/10.1007/s10934-014-9871-y.

[21] Woan K, Pyrgiotakis G, Sigmund W. Photocatalytic carbon-nanotube-TiO_2 composites. Adv Mater, **21**, 2233 (2009). https://doi.org/10.1002/adma.200802738.

[22] Safarik I, Angelova R, Baldikova E, Pospiskova K, Safarikova M. Leptothrix sp. sheaths modified with iron oxide particles: magnetically responsive, high aspect ratio functional material. Mater Sci Eng C, **71**, 1342 (2017). https://doi.org/10.1016/j.msec.2016.10.056.

[23] Papaevangelou VA, Gikas GD, Tsihrintzis VA. Chromium removal from wastewater using HSF and VF pilot-scale constructed wetlands: overall performance, and fate and distribution of this element within the wetland environment. Chemosphere, **168**, 716 (2017). https://doi.org/10.1016/j.chemosphere.2016.11.002.

[24] Chen YD, Chen WQ, Huang B, Huang MJ. Process optimization of $K_2C_2O_4$-activated carbon from kenaf core using Box–Behnken design. Chem Eng Res Des, **91**, 1783 (2013). https://doi.org/10.1016/j.cherd.2013.02.024.

[25] Zhang HB, Lin GD, Zhou ZH, Dong X, Chen T. Raman spectra of MWCNTs and MWCNT-based H_2-adsorbing system. Carbon, **40**, 2429 (2002). https://doi.org/10.1016/s0008-6223(02)00148-3.

[26] Liang Y, Zhang H, Yi B, Zhang Z, Tan Z. Preparation and characterization of multi-walled carbon nanotubes supported PtRu catalysts for proton exchange membrane fuel cells. Carbon, **43**, 3144 (2005). https://doi.org/10.1016/j.carbon.2005.06.017.

[27] Wu W, Chen W, Lin D, Yang K. Influence of surface oxidation of multiwalled carbon nanotubes on the adsorption affinity and capacity of polar and nonpolar organic compounds in aqueous phase. Environ Sci Technol, **46**, 5446 (2012). https://doi.org/10.1021/es3004848.

[28] Yang S, Li J, Shao D, Hu J, Wang X. Adsorption of Ni(II) on oxidized multi-walled carbon nanotubes: effect of contact time, pH, foreign ions and PAA. J Hazard Mater, **166**, 109 (2009). https://doi.org/10.1016/j.jhazmat.2008.11.003.

[29] Zuccaro L, Krieg J, Desideri A, Kern K, Balasubramanian K. Tuning the isoelectric point of graphene by electrochemical functionalization. Sci Rep, **5**, 11794 (2015). https://doi.org/10.1038/srep11794.

[30] Szlachta M, Wójtowicz P. Adsorption of methylene blue and Congo red from aqueous solution by activated carbon and carbon nanotubes. Water Sci Technol, **68**, 2240 (2013). https://doi.org/10.2166/wst.2013.487.

[31] Li YH, Wang S, Luan Z. Adsorption of cadmium(II) from aqueous solution by surface oxidized carbon nanotubes. Carbon, **41**, 1057 (2003). https://doi.org/10.1016/s0008-6223(02)00440-2.

[32] Wu T, Cai X, Tan S, Li H, Liu J, Yang W. Adsorption characteristics of acrylonitrile, p-toluenesulfonic acid, 1-naphthalenesulfonic acid and methyl blue on graphene in aqueous solutions. Chem Eng J, **173**, 144 (2011). https://doi.org/10.1016/j.cej.2011.07.050.

[33] Guo Y, Deng L, Li J, Guo S, Wang E, Dong S. Hemin-graphene hybrid nanosheets with intrinsic peroxidase-like activity for label-free colorimetric detection of single-nucleotide polymorphism. ACS Nano, **5**, 1282 (2011). https://doi.org/10.1021/nn1029586.